International Journal of Multiphase Flow 35 (2009) 924–932

Contents lists available at ScienceDirect

International Journal of Multiphase Flow

journal homepage: www.elsevier.com/locate/ijmulflow

An experimental investigation of roll waves in high pressure two-phase inclined pipe flows

George W. Johnson [a,*], Arnold F. Bertelsen [b], Jan Nossen [c]

[a] StatoilHydro ASA, Research Centre Porsgrunn, NO-3908 Porsgrunn, Norway
[b] University of Oslo, Department of Mathematics, Section of Mechanics, P.O. Box 1053, Blindern NO-0135, Oslo 3, Norway
[c] Institute for Energy Technology, P.O. Box 40, NO-2027 Kjeller, Norway

ARTICLE INFO

Article history:
Received 23 July 2008
Received in revised form 7 June 2009
Accepted 9 June 2009
Available online 14 June 2009

Keywords:
Gas–liquid pipe flow
Stratified flow
Stratified transition
High pressure
Roll waves
Pipe inclination

ABSTRACT

This paper examines the effects of small upward inclinations on the formation of roll waves and the properties of fully developed roll waves at high pressure conditions. A total of 984 experiments were conducted at six positive pipe inclinations $\theta = 0.00°$, $0.10°$, $0.25°$, $1.00°$, $2.50°$ and $5.00°$ using a 25 m long 10 cm i.d. pipe. Sulfur hexafluoride (SF_6) was used at 8 bara giving a gas density of 50 kg/m^3. Two independent mechanisms for the formation of roll waves were identified; (1) interaction between 2D shallow water waves and (2) a visible long wavelength instability of the stratified layer. Viscous long wavelength linear stability analysis predicted the critical liquid flow rate and liquid height for the initiation of roll waves when roll waves were formed due to the second mechanism. A simple equation from shallow water wave theory agreed with measurements for critical liquid flow rate when roll waves were formed due to the first mechanism. Shallow water wave speed agreed with critical wave speeds at transition and nonlinear wave speeds for fully developed roll waves in certain cases. The increase in interfacial friction due to the presence of large waves was compared with models from the literature.

1. Introduction

Few high pressure stratified pipe flow experiments exist in the literature due to significant expenditures and technical requirements. Experimental investigations at high pressure and small pipe inclinations are needed for the development of models which can be used for the design of offshore gas condensate transport lines. Gas transport lines consist of a number of pipe sections where each section has some degree of inclination due to the topography of the ocean floor. Condensate forms during transport as natural gas from the reservoir cools within the transport pipeline. At certain gas and liquid flow rates, instabilities in the condensate layer may develop into large roll waves or slugs which influences pressure drop and transport rates. This paper compares theoretical criteria for the formation of roll waves at small upward inclinations with observations and examines models for interfacial friction which is significant in the roll wave regime.

In general two-phase roll waves appear much like single phase hydraulic bores in downward inclined open channels as were first observed by Cornish (1934). These large waves are characterized by sharp breaking fronts and long sloping backs. In two-phase flows roll waves lead to gas–liquid mixing and are involved in the formation of slugs. Hanratty and Hershman (1961) developed long wavelength stability theory for the formation of roll waves which agreed with measurements from air–water channel flows. Bruno and McCready (1988) investigated the formation of roll waves using stability theory in air–water channel flows and determined that roll waves formed due to growing "precursor waves" which exist at the same frequency as roll waves but at much smaller gas Reynolds numbers than observed by the long wavelength analysis of Hanratty and Hershman (1961), Kordyban and Ranov (1970), Wallis and Dobson (1973) and Taitel and Dukler (1976) developed conditions for the formation of slug flows using inviscid stability analysis. This work was extended by Lin and Hanratty (1986a) to include inertia and viscous effects and was applied for the prediction the formation of slugs. At high pressure conditions Wu et al. (1987) determined that viscous long wavelength (VLW) stability theory coincided with the formation of roll waves in horizontal pipes.

VLW stability theory has been compared with the formation of roll waves and the formation of slugs in gas–liquid flows and the fact that information about nonlinearities and interaction between waves cannot be determined may provide an explanation as to why different conclusions have been made. Experimental investigations into the types of instabilities which develop into roll waves and slugs help to provide useful insight into the application of VLW stability theory in gas–liquid flows.

For small gas flow rates, Fan et al. (1993) observed that nonlinear waves having wavelengths of 8–10 cm were found to form

* Corresponding author. Tel.: +47 41411525; fax: +47 35924738.
E-mail address: geoj@statoilhydro.com (G.W. Johnson).

0301-9322/$ - see front matter © 2009 Elsevier Ltd. All rights reserved.
doi:10.1016/j.ijmultiphaseflow.2009.06.003

slugs in a 9.5 cm horizontal pipe at atmospheric conditions. The small amplitude long wavelength waves predicted by VLW stability theory were not the source of slug formation in this investigation. At large gas flow rates and sufficient liquid depths, Andritsos (1986) found that interaction between waves eventually resulted in a slugging pattern which could not be accounted for using VLW stability analysis. For small downward inclined pipe flows, Woods et al. (2000) determined that the waves observed by Fan et al. (1993) were damped and that long wavelength small amplitude waves formed slugs which gave support for the prediction of slug formation using VLW stability theory.

Motivated by the limitations of VLW stability theory, a different modelling approach was suggested by Ruder et al. (1989) which focused on the conditions necessary for the stability slugs. This approach was further developed by Hurlburt and Hanratty (2002) who suggested that if the liquid layer is determined to be unstable using VLW stability theory, the final outcome (i.e. roll waves or slugs) could be determined using slug stability criteria. Soleimani and Hanratty (2003) investigated the approach of Hurlburt and Hanratty (2002) for air/water flows in a 2.54 cm i.d. pipe and made detailed observations about the critical liquid depth and critical flow rates necessary for the formation of roll waves and slugs. It was determined that at low superficial gas velocities VLW stability theory predicted the formation of roll waves, but if the liquid height was sufficiently large roll waves could develop directly into slugs. For large gas flow rates slug formation was caused by roll wave coalescence as first observed by Lin and Hanratty (1986a). Based on differences between the approach of Hurlburt and Hanratty (2002) with observations, Soleimani and Hanratty (2003) suggested that a criterion for the initiation of roll wave coalescence was needed as well as a criterion for slug formation from pseudo-slugging. Experimental investigations using inclined pipes include Beggs and Brill (1973), Barnea et al. (1980), Ferschneider et al. (1985) and Espedal (1998) where relatively large liquid flow rates were required for slug formation at negative pipe inclinations and relatively small liquid flow rates resulted in slug formation at positive inclinations compared with horizontal flows.

The "two-fluid model", which is the basis for stratified flow models, depends on a model for friction at the gas–liquid interface. Large waves are known to increase interfacial friction compared with smooth stratified flows as reported by for example Hanratty (1991) and Andritsos (1986). A number of researchers including Miya et al. (1971), Cheremisinoff and Davis (1979), Andreussi and Persen (1987), Andritsos and Hanratty (1987), Kowalski (1987) and Biberg (2002) developed empirical models for the relative increase in interfacial friction for wavy two-phase stratified flows. The model by Andritsos and Hanratty (1987) for atmospheric flows was compared with the data from this investigation. This paper provides a unique set of high pressure data at upward pipe inclinations. New observations were made about roll wave formation and fully developed roll waves. Observations of roll waves at high pressure conditions gave some surprising results when compared with theory.

2. Theory

2.1. Momentum equations

The "two-fluid" model equations provide the basis for the theoretical analysis which was used for determining transition criteria and determining the friction at the interface. Fig. 1 can be used as a reference for the variables in the equations. A shallow water assumption was made so that the pressure variation p at a given x-location along the pipe axis was given by

$$p_k = P_{ik} + \rho_k(h(x) - y)g\cos\theta, \tag{1}$$

where h is the liquid height, ρ the fluid density, g the acceleration of gravity, P_i the pressure at the interface and θ the pipe angle of inclination. Throughout the text, the index i represents the interface and k represents the gas phase when $k = g$ and liquid phase when $k = l$.

The mean axial velocities are given as

$$U_k = A_k^{-1}\int_{A_k} u_k\,dA, \tag{2}$$

where u represents the local axial velocity component.

The mass and momentum conservation equations, using the shallow water assumption, are given below

$$\frac{\partial}{\partial t}(\rho_k A_k) + \frac{\partial}{\partial x}(\rho_k A_k U_k) = 0, \tag{3}$$

$$\frac{\partial}{\partial t}(\rho_l A_l U_l) + \frac{\partial}{\partial x}\left(\Gamma_l \rho_l A_l U_l^2\right) = -A_l\frac{\partial P_{li}}{\partial x} - \rho_l A_l g\cos\theta\frac{\partial h}{\partial x} - \rho_l A_l g\sin\theta - \tau_l S_l + \tau_i S_i, \tag{4}$$

and

$$\frac{\partial}{\partial t}(\rho_g A_g U_g) + \frac{\partial}{\partial x}\left(\Gamma_g \rho_g A_g U_g^2\right) = -A_g\frac{\partial P_{gi}}{\partial x} - \rho_g A_g g\cos\theta\frac{\partial h}{\partial x} - \rho_g A_g g\sin\theta - \tau_g S_g - \tau_i S_i. \tag{5}$$

For the equations above, the shape factors are given by Γ, the shear stresses are given by τ, A represents the cross-sectional area and S represents the perimeter over which τ acts (see Fig. 1).

The shape factors are defined as

$$\Gamma_k = \frac{1}{A_k U_k^2}\int_{A_k} u_k^2\,dA. \tag{6}$$

The gas and liquid shear stresses in Eqs. (4) and (5) are modelled as

$$\tau_k = \frac{1}{8}\rho_k f_k U_k^2, \tag{7}$$

where the friction factors $f = f(Re)$ depend on the following Reynolds number given by:

$$Re_k = \rho_k U_k D_k/\mu_k, \tag{8}$$

where μ represents dynamic viscosity and D_k the hydraulic diameters defined as

$$D_l = \frac{4A_l}{S_l}, \quad D_g = \frac{4A_g}{(S_i + S_g)}. \tag{9}$$

Shear stress at the interface is modelled as

$$\tau_i = \frac{1}{8}\rho_g f_i(U_g - U_l)|(U_g - U_l)|. \tag{10}$$

The friction at the interface is often represented by

$$f_i = \phi f_g, \tag{11}$$

where ϕ is a factor which accounts for the increase in interfacial friction relative to the gas wall friction. The following model of Haaland (1983) for the friction factor in Eqs. (7) and (10),

$$\frac{1}{\sqrt{f_k}} = -1.8\log\left[\frac{6.9}{Re_k} + \left(\frac{\epsilon}{3.7D}\right)^{1.11}\right], \tag{12}$$

accounts for pipe surface roughness through the factor ϵ.

Assuming incompressible fluids, the pressure terms in Eqs. (4) and (5) are related using the following approximation:

$$P_{ig} - P_{il} = \sigma\frac{\partial^2 h}{\partial x^2}, \tag{13}$$

where σ represents the surface tension coefficient.

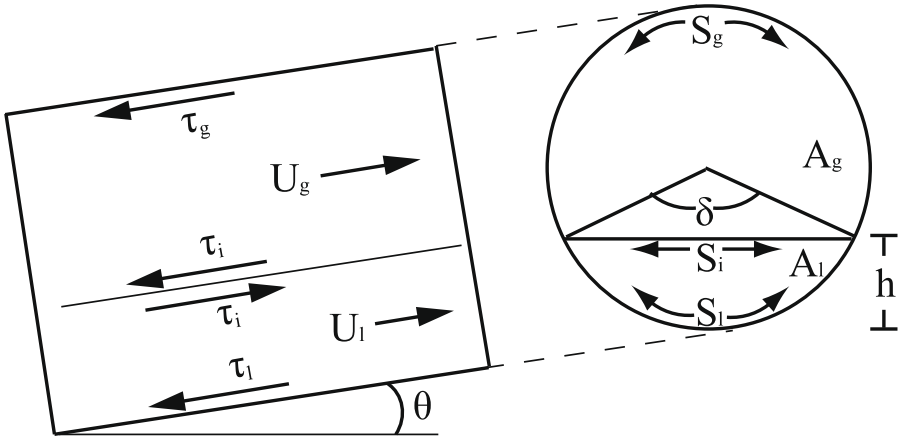

Fig. 1. Sketch of the gas and liquid velocities U_g and U_l in the cross-sectional areas A_g and A_l, respectively. The gas, liquid and interfacial shear stresses τ_g, τ_l and τ_i act on the pipe perimeters given by S_g, S_l and S_i, respectively. The angle measured from the center of the pipe to the gas–liquid interface is given by δ and the pipe inclination is given by the angle θ.

2.2. Viscous long wavelength stability theory

As described by Watson (1989), the VLW stability equations can be derived from the conservation equations (Eqs. (3)–(5)) by assuming plug flow, i.e. $\Gamma = 1$ as well as $P_{ig} \approx P_{il}$. Introducing a relative coordinate system, where $X = x - Ct$, Eq. (3) becomes

$$\frac{\partial}{\partial X}(U_k - C)A_k = 0. \tag{14}$$

Subtracting Eq. (4) from (5) gives

$$N\frac{dh}{dX} = T, \tag{15}$$

where

$$N = \Delta\rho g H\cos\theta - \rho_l(U_l - C)^2 - \rho_g\left(\frac{A_l}{A_g}\right)(U_g - C)^2, \tag{16}$$

and

$$T = H\left[-\Delta\rho g\sin\theta + \left(\frac{1}{A_l} + \frac{1}{A_g}\right)\tau_i S_i + \frac{1}{A_g}\tau_g S_g - \frac{1}{A_l}\tau_l S_l\right], \tag{17}$$

in the relative coordinate system. The following three conditions represent VLW stability criterion for two-phase pipe flows:

$$T = N = \frac{dT}{dh} = 0, \tag{18}$$

where after differentiating Eq. (17) with reference to h, the variables are time averaged properties, i.e. $(h, U, \ldots) \rightarrow \left(\overline{h}, \overline{U}, \ldots\right)$. A formal derivation of VLW stability theory can be found in for example Woods et al. (2000), which is equivalent to the conditions in Eq. (18).

2.3. Shallow water wave theory

In addition to comparing the complete VLW stability theory with the formation of roll waves, a simplification to Eq. (16) was made which results in the well known equation for shallow water wave (SWW) speed which can be applied to pipe flows. A brief description of SWW theory, as found in Whitham (1999), follows.

SWW speed for single phase flows in an infinitely wide open channel of depth h is given by

$$C = U_o \pm \sqrt{gh}, \tag{19}$$

where U_o is the mean liquid speed in the x-direction defined by

$$U_o = \frac{1}{h}\int_0^h u\,dy, \tag{20}$$

and $u(y)$ is the local x velocity component. The condition $h \ll \lambda$, where λ represents wavelength, must be fulfilled for Eq. (19) to satisfy the model assumptions. To apply Eq. (19) for pipe flows the characteristic liquid depth $H \equiv A_l/S_i$ was chosen and the velocity U_o for a channel is replaced by the cross-sectionally averaged axial liquid velocity U_l for a pipe given by Eq. (2). Substituting h and U_o with H and U_l, respectively, the SWW speed for pipe flows is

$$C = U_l \pm \sqrt{gH\cos\theta}, \tag{21}$$

where $\cos\theta$ accounts for positive pipe inclinations. Focusing on the waves which progress in the direction of the flow, Eq. (21) can be rearranged to obtain the following equation:

$$U_l = C - \sqrt{gH\cos\theta}, \tag{22}$$

which can be expressed with the superficial liquid velocity

$$U_{sl} = \alpha_l\left(C - \sqrt{gH\cos\theta}\right), \tag{23}$$

where $\alpha_l \equiv A_l/A$ represents liquid holdup. Expressing Eq. (21) using the superficial liquid velocity gives

$$C = \alpha_l^{-1}U_{sl} + \sqrt{gH\cos\theta}. \tag{24}$$

Alternatively, Eqs. (21)–(24) can be obtained by setting $C = U_g$ in Eq. (16) where $\sqrt{1 - \rho_g/\rho_l} \approx 1$.

2.4. Equilibrium flows

For equilibrium steady state conditions, Eqs. (3)–(5) become

$$0 = \frac{\partial}{\partial x}(\rho_k A_k U_k), \tag{25}$$

$$0 = -A_g\left(\frac{dP_i}{dx}\right) - \tau_g S_g - \tau_i S_i - A_g\rho_g g\sin\theta, \tag{26}$$

$$0 = -A_l\left(\frac{dP_i}{dx}\right) - \tau_l S_l + \tau_i S_i - A_l\rho_l g\sin\theta. \tag{27}$$

The sum of Eqs. (26) and (27) gives

$$-\left(\frac{dP_i}{dx}\right) = (\alpha_l\rho_l - \alpha_g\rho_g)g\sin\theta + \tau_l\frac{S_l}{A} + \tau_g\frac{S_g}{A}, \tag{28}$$

where $\alpha_k = A_k/A$. Eq. (28) will be used to determine a theoretical pressure drop by using Eq. (7) for the shear stresses and supplying the right-hand side with measured mean liquid depth.

The value for $\phi = f_i/f_g$ can be calculated from Eqs. (26) and (27) together with measured mean liquid heights. Inserting Eq. (11) into Eq. (10) then subtracting Eq. (26) from Eq. (27) and solving for ϕ gives

$$\phi = 8\left(\frac{\Delta\rho g \sin\theta\alpha_g\alpha_l A + \frac{1}{8}\rho_l f_l U_l^2 S_l \alpha_g - \frac{1}{8}\rho_g f_g U_g^2 S_g \alpha_l}{(f_g\rho_g(U_g - U_l)|(U_g - U_l)|)S_i}\right). \quad (29)$$

Andritsos and Hanratty (1987) suggested the following empirical correlation for ϕ based on experimental data:

$$\phi = 1 + 15\left(\frac{h}{D}\right)^{1/2}\left(\frac{U_{sg}}{U_{sgt}} - 1\right), \quad (30)$$

where

$$U_{sgt} = 5\left(\frac{\rho_{ga}}{\rho_g}\right)^{1/2}, \quad (31)$$

and ρ_{ga} is the gas density at atmospheric pressure.

3. Experimental set-up and data analysis

The number of experiments at θ = 0.00°, 0.10°, 0.25°, 1.00°, 2.50° and 5.00°, as measured from the horizontal plane, was 206, 214, 219, 163, 115 and 67, respectively. The 10 cm i.d. pipe consisted of two pipe sections (10 m and 15 m long) which were joined by a smooth flexible coupling. Both sections were inclined equally such that the effective length was 25 m. The length to diameter ratio was 250. Pipe inclination was measured using an inclinometer with an accuracy of 0.01°. A 3 m section of the pipe was made of transparent PVC which allowing visual observations and digital video recording of the flow. The pipe roughness $\epsilon = 5 \times 10^{-5}$ m was determined using single phase gas at a number of flow rates. The operating ranges of the flow meters are given in Table 1 and an overview of the experimental set-up is shown in Fig. 2.

Measurements of gas density gave a value of $\rho_g = 50$ kg/m^3 and tables indicated a dynamic viscosity of $\mu_g = 1.61 \times 10^{-5}$ kg/ms. Tables for water at 20 C indicated a density of $\rho_l = 998$ kg/m^3,

Table 1
Overview of the operating ranges of the laboratory equipment.

Measurement	Operating range	Measurement device
U_{sl}	0.01–1.5 m/s	Fischer & Porter Electromagnetic Flow meter Type 10 Dx 3311A
U_{sg}	0.1–15 m/s	Instrument DN80 Turbine meter Type Q-75-F (25–400 m^3/h)
U_{sg}	0.1–1.5 m/s	Fischer & Porter Vortex meter Type 10V-1
Differential pressure	0–2000 Pa	Fuji Electric Differential Pressure Type FHC W11 W1 AKCAY
Holdup	–	Two-energy broad beam γ-densitometer

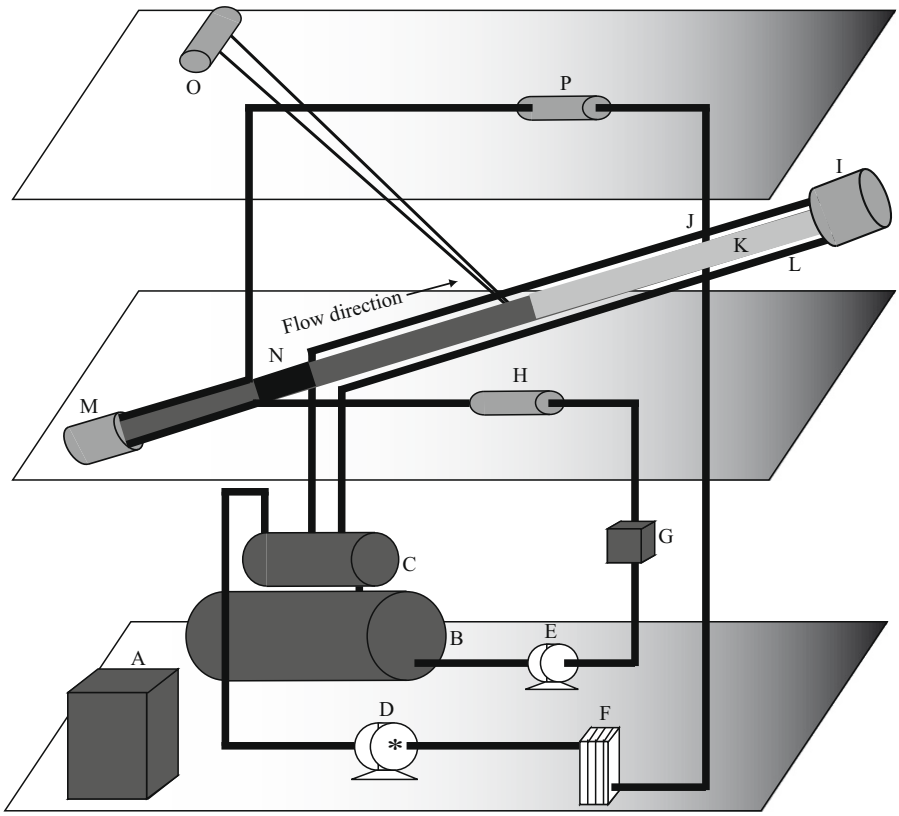

Fig. 2. Sketch of the three-story laboratory. G. (gas), L. (liquid). (A) Control panel; (B) main separator; (C) Pre-separator; (D) G. comp. pump; (E) L. centrifugal pump; (F) G. plate heat exchanger; (G) L. heat exchanger; (H) L. flow rate meter; (I) inline separator; (J) G. return line; (K) transparent pipe section; (L) L. return line; (M) pipe inlet; (N) flexible section; (O) winch; and (P) G. flow rate meter.

Table 2
Overview of the instruments which were used to calculate the results. Wave probes given by (wp), γ-densitometers given by (γ) and pressure transducers given by dP.

Instrument	wp1	wp2	wp3	wp4	γ_1	γ_2	dP_1	dP_2	dP_3
Holdup					×	×			
Pressure gradient							×	×	×
Wave speed	×	×	×	×					
Wave height	×	×	×	×	×	×			
Wavelength	×	×	×	×	×	×			

and $\mu_l = 9.98 \times 10^{-4}$ kg/ms. The gas was held at ≈20 C using a counter-current plate heat exchanger. A small amount of sodium sulfate was added to the water (350 mg/L) to maximize the range of the four conductivity wave probes.

Measurement instrumentation was located in the final ≈8 m section of the pipe. Pressure drop was recorded using three[1] differential pressure transducers at 3 Hz which had an accuracy of 0.1% FSO and a range of 2000 Pa. Two broad beam γ-densitometers and four wave probes recorded liquid height at 50 Hz. The γ-densitometers had an accuracy of ±0.02 (absolute).

Wave properties and variations in liquid height were measured using a liquid conductance technique. Wave probes measured conductivity between two 400 μm diameter vertical platinum wires which were separated at the pipe centerline by a distance of 3 mm. An electrical signal was applied to one of the wires and the level of conductivity measured. Conductivity was linearly dependent on the fraction of liquid between the wires. Each individual wave probe was calibrated against the γ-densitometers and the conductance measurements were converted into an equivalent h/D where the liquid height h was measured from the bottom of the pipe.

Wave probe measurements were used for the determination of wave amplitude, speed and frequency. The reported values for mean liquid height were determined exclusively using the γ-densitometers. Table 2 indicates which instruments were used to obtain holdup, wave speed, pressure drop, etc. Details regarding the relative placement of the pressure transducers, wave probes and γ-densitometers are given in Fig. 3. Additional details of the experimental set-up can be found in Electronic Annex 2.

3.1. Data analysis

Details describing the calculations which were used to determine mean values for pressure drop, liquid height, wave speed, wavelength and wave height are given in this section. In general, data from individual instruments were averaged to give an aggregate (final) value for each experiment. For example mean holdup α_l was determined by averaging the time averaged values reported by each of the two γ-densitometers, i.e.

$$\alpha_l = \frac{1}{2}\left(\sum \overline{\alpha_{l\gamma 1}} + \overline{\alpha_{l\gamma 2}}\right), \tag{32}$$

where $\overline{\alpha_{l\gamma 1}}$ represents a time averaged value for holdup from the first γ-densitometer. Data from the pressure transducers were averaged using the same approach.

Andritsos (1986), Strand (1993) and others calculated wave height using

$$h_s = 2\sqrt{2}\sigma_s, \tag{33}$$

where σ_s represents the RMS standard deviation of the liquid height time trace $h(t)$ from the wave probes and γ-densitometers. An aggregate mean wave height was calculated for each experiment by using Eq. (33) for each time trace and averaging the results.

[1] For some experiments only two pressure transducers where available.

Cross-correlation series require the simultaneous liquid height time traces from any two separate instruments. The following expression for the normalized cross-correlation series was used:

$$\xi(\Delta t) = \frac{\sum_j \left[\left(h_x(j) - \bar{h}_x\right)\left(h_y(j-\Delta t) - \bar{h}_y\right)\right]}{\sqrt{\sum_j \left(h_x(j) - \bar{h}_x\right)^2}\sqrt{\sum_j \left(h_y(j) - \bar{h}_y\right)^2}}, \tag{34}$$

where j represents a discrete point in time, Δt represents a time delay and h_x and h_y represent liquid height time traces which were obtained from instruments x and y. The maximum value of ξ gave the unique length of time τ_d that a wave traveled between instruments. The wave speed was determined using $C = L/\tau_d$, where L represents the length between two instruments. Given that Eq. (34) was normalized, the degree of correlation was calculated using the magnitude of ξ where $0 \leqslant \xi(\Delta t) \leqslant 1$. A value of $\xi = 1$ represents a perfect correlation. Seven cross-correlations were performed for each experiment and these values were averaged to determine an aggregate mean wave speed.

Wavelength was found using $\lambda = C/f_d$, where the dominating frequency f_d was obtained from power spectra using the method described below. Discrete Fourier transforms were calculated from the liquid height time traces of the wave probes and γ-densitometers using

$$G_\kappa = \sum_{t=0}^{N-1} h_t \exp\left(\frac{-2\pi j t \kappa}{N}\right) \quad \text{for } \kappa = 1, \ldots, N-1, \tag{35}$$

where, $j = \sqrt{-1}$, $N = 512$ is the number of time-trace samples, h_t represents the liquid height at time t and κ represents a discrete frequency. The power spectral density function $\Pi(\kappa)$ was calculated using

$$\Pi(\kappa) = \frac{1}{N^2}\left[|G_\kappa|^2 + |G_{N-\kappa}|^2\right] \quad \text{for } \kappa = 1, \ldots, (N/2-1), \tag{36}$$

where the magnitude of Π represented the specific energy of the time-trace measurements in units of mm^2 s^{-2}. The value for κ, where $\Pi(\kappa)$ was greatest, gave the dominating frequency using $f_d = \kappa/(NT)$ where $N = 512$, the period $T = 1/f_m$ and $f_m = 50$ Hz. The spectral functions in Fig. 4 were normalized with the square of the RMS standard deviation from the time series.

4. Results and comparisons

4.1. The formation of roll waves

Four types of waves were observed; (1) capillary waves, (2) 2D waves, (3) 3D waves and (4) roll waves. Capillary waves had wavelengths which were in the order of 10^{-3} m and small amplitudes <5 mm. Large 2D waves having wavelengths $\lambda \leqslant 0.75$ m were observed at low gas rates and angles $\leqslant 1.00°$. 3D waves had short wavelengths and relatively large amplitudes. These waves appeared as chaotic disturbances at the interface making it difficult to visually distinguish between individual 3D waves. A similar description of these waves was given by Espedal (1998) based on observations at atmospheric pressure. Roll waves are easily recognized due to low frequencies, large wave speed, large amplitudes and characteristic breaking fronts. Different types of waves existed simultaneously near the roll wave transition region.

The transition to roll waves occurred due to two separate mechanisms: (1) interaction between 2D waves at low gas rates and (2) a long wavelength instability of the liquid layer in the presence of 3D waves at large gas rates. Additionally 2D waves did occasionally form breaking fronts spontaneously without any obvious wave interaction. The transition from 3D waves to roll waves occurred at higher gas rates than those which allowed 2D waves and can be explained as follows. A shallow liquid film having 3D waves,

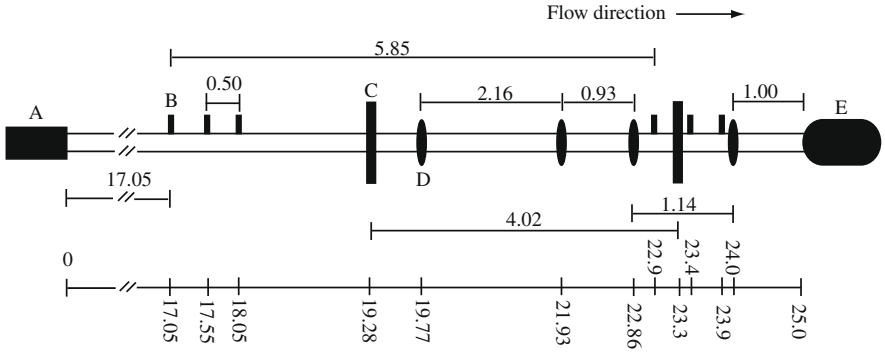

Fig. 3. The position of the pressure sample points (B), γ-densitometers (C), wave probes (D) and outlet separator(E), measured in meters from the inlet (A).

developed relatively thick regions which over time grew in amplitude until eventually forming breaking roll waves. The distance between the thick regions was large, i.e. ≈100 pipe diameters.

Power spectra were used to identify 2D waves and roll waves. The power spectra in Fig. 4 were obtained at flow rates near the transition between 2D waves and roll waves in horizontal flows. By comparison 2D waves had frequencies of ≈2 Hz and lower energy levels than roll waves which had frequencies <1 Hz. Based on the power spectra, roll waves appeared to develop from "precurssor waves" as first noted by Bruno and McCready (1988). These precurssor waves are believed to be 2D waves which interact at a frequency below the primary frequency of the 2D wave train as seen in Fig. 4.

4.2. Linear long wavelength stability theory compared with observations

Critical liquid height, superficial liquid velocity and wave speed were compared with corresponding theoretical values from VLW stability theory using the conditions in Eq. (18). Solutions to VLW allowed the determination of theoretical values for U_{sl}, h/D and C when U_{sg} and corresponding experimental values for ϕ (see Eq. (29)) were specified. Critical superficial liquid velocity and wave speed were compared with the SWW equations given by Eqs. (23) and (24), respectively.

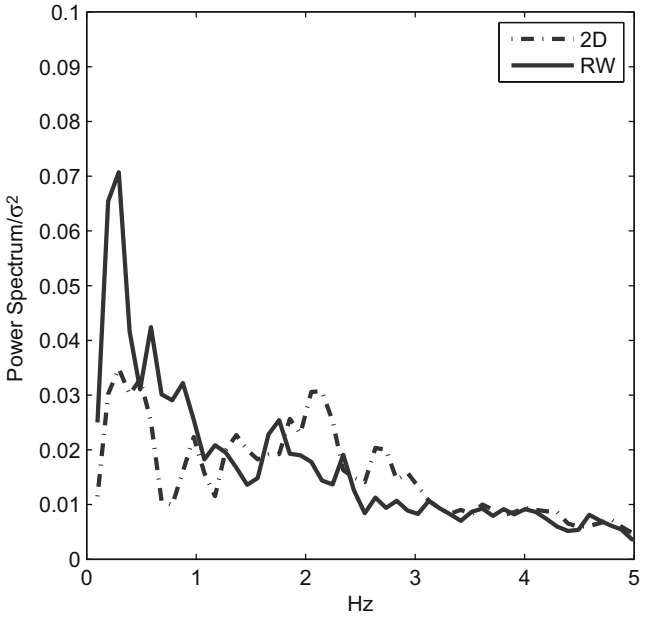

Fig. 4. Power spectra of 2D waves ($U_{sg} = 0.726$ m/s, $U_{sl} = 0.225$ m/s) and roll waves ($U_{sg} = 0.726$ m/s, $U_{sl} = 0.257$ m/s) in horizontal flow.

Both VLW stability theory and the SWW equations matched data for the critical superficial liquid velocity. However, VLW stability theory over predicted U_{sl} at the lowest U_{sg} values where 2D waves formed roll waves. Results from VLW stability theory and SWW theory can be seen in Fig. 5 and Figs. 1–6 in Electronic Annex 3. Solutions to Eq. (23) gave the theoretical critical superficial liquid velocity when measured values for C and h/D were used. SWW theory given by Eq. (23) gave better results than VLW stability theory when determining critical U_{sl} for the majority of the experiments.

An investigation into the magnitude of the liquid shape factor was made using a method similar to Woods (1998). Values for U_{sg}, U_{sl} and the measured value for ϕ and h/D were given as input data to Eqs. (16)–(18) where the following correction to Eq. (16) was made:

$$(U_l - C)^2 \rightarrow \left(U_l^2 - 2\Gamma_l U_l C + \Gamma_l C^2\right). \tag{37}$$

Solving Eqs. (16)–(18) using Eq. (37) and the input variables allowed the determination of Γ_l and C.

Values for the liquid shape factor are shown in Fig. 7. The magnitude of the shape factor was in accordance with the findings of Woods et al. (2000), however, the same dependence of the liquid shape factor on liquid Reynolds number was not found. Low Reynolds numbers for the gas phase gave large liquid shape factors. The liquid shape factor did not depend on the liquid Reynolds number as it did the gas Reynolds number. The large gas density of these experiments may explain why the liquid shape factor was found to have a greater dependency on the gas Reynolds number than liquid Reynolds number.

The approach of assuming plug flow, i.e. $\Gamma_l = 1$ and the alternative approach of determining $\Gamma_l \neq 1$ gave similar results for linear wave speed using VLW stability theory. More surprisingly though was the level of agreement between Eq. (24) and measurements. Although Eq. (24) is identical in form to single phase SWW theory, the fact that the liquid layer is much lower in two-phase flows causes the local liquid velocity $U_l = U_{sl}/\alpha_l$ to be large. This in turn results in relatively large theoretical wave speeds which agree with measured wave speeds (see Eq. (21)). A comparison of predicted wave speeds with measured wave speeds at transition can be seen in Fig. 6 and Figs. 13–19 in Electronic Annex 3. Theoretical waves speeds under predicted measured wave speeds by <10% and $U_{sg} < 3$ m/s for $\theta \leqslant 1.00$. At larger inclinations and superficial gas velocities, differences between theory and measurements increased.

The ratio $\phi = f_i/f_g$ at transition was on average ≈4 for horizontal flows as determined by Eq. (29). A mean value of $\phi \approx 7$ was found for $\theta \geqslant 2.50°$. Values for ϕ had a significant influence on the predictions obtained from VLW stability analysis. Wu et al. (1987) used

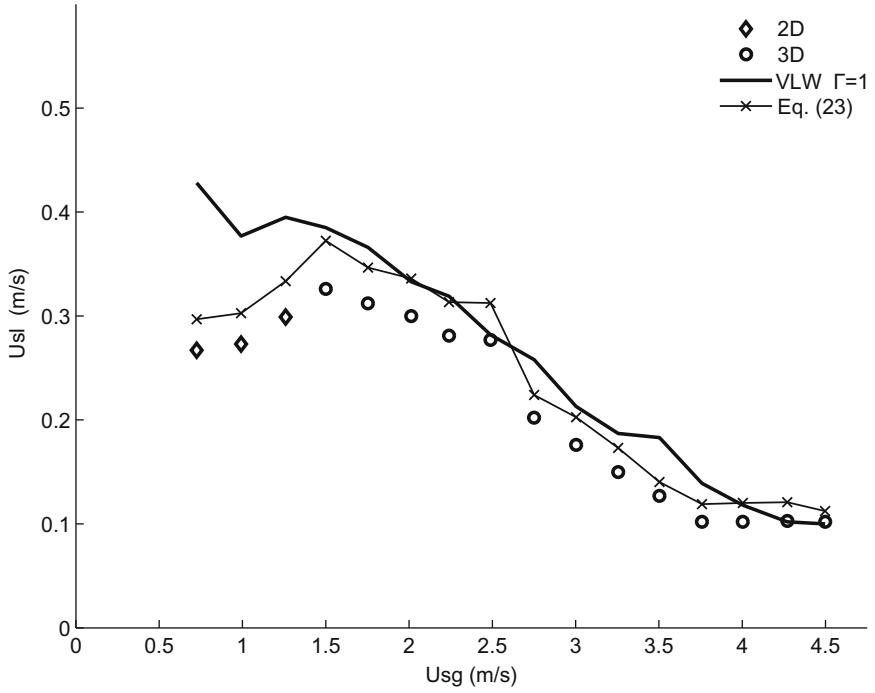

Fig. 5. The critical superficial liquid velocity for horizontal flows at the formation of roll waves.

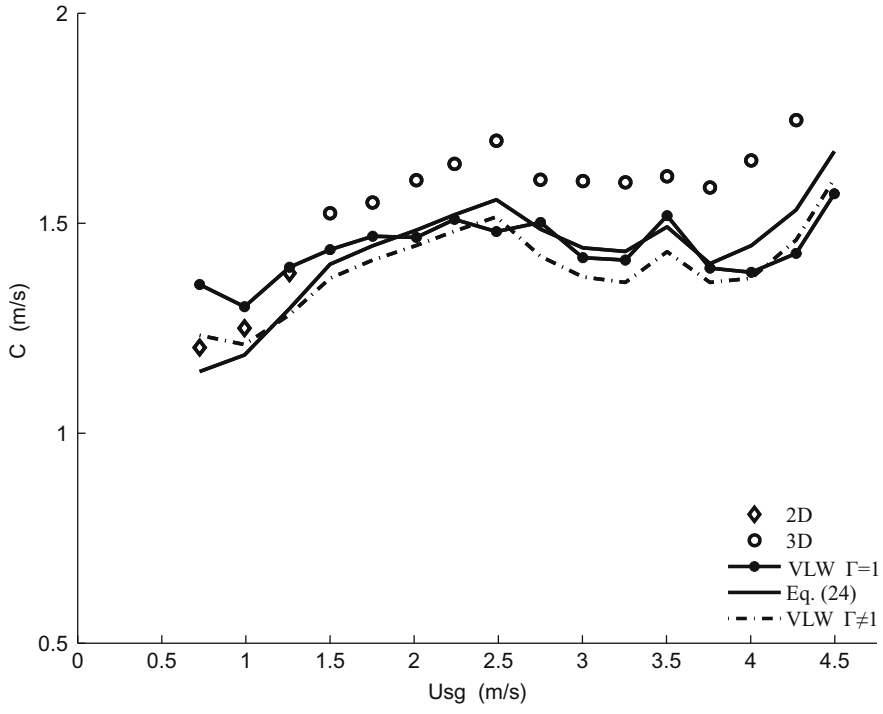

Fig. 6. The critical wave speed for horizontal flows at the formation of roll waves.

the assumption $\phi = 1$, which was satisfactory for horizontal flows, but large discrepancies would have been found had this assumption been applied for upward inclinations where $\phi \approx 7$.

4.3. Fully developed roll waves

Fully developed roll waves were observed in 754 experiments. Tables of data from each experiment are given in Electronic Annex 4. Pressure drop, liquid height, wave speed and ϕ (Eq. (29)) was compared with theoretical models for fully developed roll waves from the literature. A model for nonlinear roll waves by Johnson et al. (2009) was compared with wave speed, pressure drop and mean liquid height. The relative increase in interfacial friction associated with the presence of waves was compared with models by Andritsos (1986) and Johnson et al. (2009). In addition to the high pressure data from this investigation, data from Andritsos (1986) was used to compare Eq. (24) with measured wave speeds at atmospheric conditions.

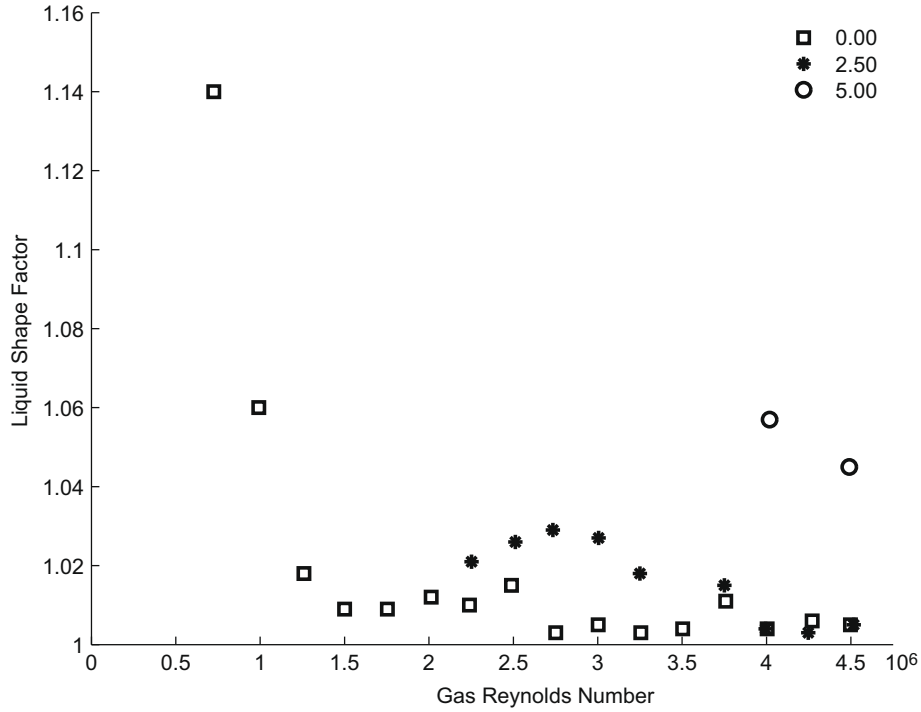

Fig. 7. The magnitude of the liquid shape factor using VLW stability theory at different angles and superficial gas velocities.

A number of wave speeds were reported in Andritsos (1986) which were compared with Eq. (24). Air and water was used in a 9.53 at atmospheric pressure cm i.d. horizontal pipe. Six experiments were labeled as 2D waves and seven experiments were labeled as large amplitude waves (roll waves). The measured 2D wave speeds differed from Eq. (24) by 4.1% and the measured roll wave speeds differed by 0.4% on average. The results indicate that at atmospheric conditions Eq. (24) predicts the wave speeds for fully developed waves if mean liquid height is known. Greater differences were seen when comparing Eq. (24) with wave speeds at high pressure conditions. The measured roll wave speeds differed from Eq. (24) by ≈11% for $\theta \leqslant 0.25°$, ≈15% for $\theta = 1.00°$ and 27% for $\theta \geqslant 2.50°$. The difference between the wave speeds at atmospheric pressure and high pressure may be attributed to the shape of the waves and/or the levels of gas dispersion in the liquid layer.

The measured interfacial friction for horizontal flow was compared with an empirical model of Andritsos (1986) given by Eq. (30). The value ρ_{ga} was needed to determine U_{sgt} (see Eq. (31)). From tables the density of SF_6 at atmospheric pressure is $\rho_{ga} = 6.164\ \mathrm{kg/m^3}$ which gives $U_{sgt} = 1.76\ \mathrm{m/s}$. According to Andritsos (1986), for U_{sg} values lower than U_{sgt}, ϕ should be set to unity. However, values for $\phi \approx 1$ were not observed except for smooth stratified flows which were only seen at the very lowest flow rates for horizontal flows. At the observed transition to roll waves the interfacial friction was 4–7 times larger than smooth stratified flow. For fully developed roll waves the average value for ϕ is given in Table 3. The model of Andritsos (1986) compared well for $U_{sg} \geqslant 3.0$ and $U_{sl} \leqslant 0.40$ where $6 \leqslant \phi \leqslant 12$ for horizontal flows.

Table 3
Ratio between the gas and interfacial friction factors for roll waves.

	0.00	0.10	0.25	1.00	2.50	5.00
Minimum	3.86	2.59	4.91	5.53	9.17	9.14
Maximum	19.23	18.40	13.94	17.80	24.98	48.66
Mean	9.37	9.17	9.22	11.16	16.75	24.35

An indication of the accuracy of Eq. (29) was estimated by comparing Eq. (28) with measurements for mean pressure drop since both of these equations are dependent on the model for the shear stresses (see Eq. (7)). Using Haaland's model for the friction factors the theoretical pressure drop was on average ≈20% less than the measured pressure drop. This can be attributed to droplets which adhered to the pipe wall in the gas region at large flow rates causing an increase in effective surface roughness beyond the inherent surface roughness of the pipe wall. At the lowest gas and liquid flow rates, where pressure drop was least, the relative accuracy of the pressure transducers became important. Based on these factors, a high degree of accuracy of for example ⩽10% using Eq. (29) cannot be expected in many cases.

According to the measurements, mean liquid height decreased with increasing U_{sg} and increased with increasing U_{sl} while mean pressure drop increased monotonically with U_{sl}, U_{sg} and pipe inclination. For the majority of experiments roll wave amplitudes increased with U_{sl} and decreased with U_{sg} as might be expected. However, at the largest gas velocities ⩾4.00 m/s wave amplitudes decreased with increasing U_{sl} which can be attributed to one of the following:

(i) the wave crests reached the top of the pipe wall and slugs formed,
(ii) the wave crests were atomized by gas shear and reduced in size.

In the first case, increases in U_{sl} could lead to increases in mean liquid height which combined with the wave amplitude will eventually reach the top of the pipe. For the second case atomization of the wave crests into water droplets due to high shear from the gas flow results in smaller wave amplitudes. Visual observations revealed that droplets were torn from the crests of roll waves at nearly all flow rate combinations. The large density of the gas resulted in large interfacial shear which eroded the wave crests where interfacial shear was largest. Therefore a criterion for the formation of slugs at high pressure conditions should account for

atomization of wave crests which delays the transition from roll waves to slug flows. Given that the focus of this study was roll waves, those interested in slug formation at high pressure conditions should see Kristiansen (2004) who performed experiments in horizontal pipes. Figures illustrating waves with a high degree of atomization can be found in Electronic Annex 1.

A roll wave model was developed by Johnson et al. (2009) which involves solving a set of five nonlinear equations simultaneously. The solution consists of the following five unique roots to the equations C, h/D, h_m/D, h_d/D and ϕ where h_m/D and h_d/D are the normalized liquid height at the trough and crest, respectively. The pressure drop and wavelength are determined by integrating from the trough to the crest of the wave. Close quantitative agreement was found for mean pressure drop, ϕ and the mean liquid height for $\theta \leqslant 1.00^\circ$. Wave speed was under predicted by ≈20% at pipe inclinations $\leqslant 1.00^\circ$ and ≈40% at larger inclinations. The model predicted wave amplitudes for $\theta \leqslant 0.25^\circ$. Therefore the model gives close quantitative agreement with fully developed roll waves at high pressure conditions for small inclinations. For relatively large pipe inclinations gas dispersion, droplet formation and non-uniform velocity profiles may need to be included in the model.

5. Summary and conclusions

Two mechanisms for roll wave formation were identified in the experimental investigation (1) interaction between 2D shallow water waves and (2) a visible long wavelength instability of the stratified layer having 3D surface waves. In agreement with Wu et al. (1987), VLW stability analysis predicted the formation of roll waves in horizontal gas–liquid pipe flows at high pressure conditions. Predictions using VLW stability theory were particularly good at large gas flow rates where the long wavelength instability formed roll waves. For small gas flow rates VLW stability theory did not agree as well where the formation of roll waves was attributed to interaction between 2D waves. The interfacial friction was larger with greater pipe inclinations at the formation of roll waves compared with horizontal flows. It was important to include the relative increase in interfacial friction for the larger inclinations to allow VLW predictions of the critical wave speed, liquid height and superficial liquid velocity when using VLW stability theory.

Shallow water wave (SWW) theory, which represents a simplification of VLW stability theory, predicted wave speed and critical superficial liquid velocity at least as well as VLW stability theory for the formation of roll waves. In many cases VLW correctly predicted liquid height but underpredicted wave speed. This was true even when accounting for the liquid shape factor in VLW stability theory. Using a method similar to Woods (1998), it was shown that the dependence of the liquid shape factor on gas superficial velocity was greater than the dependence on liquid superficial velocity at high pressure conditions. The magnitude of the liquid shape factor was large at lower gas superficial velocities and decreased for larger gas superficial velocities.

In accordance with earlier investigations, the presence of fully developed roll waves were found to increase interfacial friction at the gas–liquid interface. A model by Andritsos (1986) was compared with measurements from horizontal flows which predicted the increase in interfacial friction for large superficial gas velocities and low superficial liquid velocities. A nonlinear wave model by Johnson et al. (2009) predicted the increase in interfacial friction for horizontal flows and flows at upward inclinations. The pressured drop, mean liquid height and wave speed for fully developed roll waves agreed with measurements for small inclinations, but significant differences were seen at large pipe inclinations. SWW theory under predicted wave speeds for fully developed roll waves at high pressure conditions, but did predict wave speeds for fully developed waves at atmospheric conditions which were reported in Andritsos (1986). Therefore, roll waves at high pressure conditions had comparatively large wave speeds in relation to roll waves at atmospheric flows due to the influence of the dense gas phase at high pressure conditions.

Appendix A. Supplementary data

Supplementary data associated with this article can be found, in the online version, at doi:10.1016/j.ijmultiphaseflow.2009.06.003.

References

Andreussi, P., Persen, L.N., 1987. Stratified gas–liquid flow in downwardly inclined pipes. AIChE J. 13, 565–575.

Andritsos, N., 1986. Effect of pipe diameter and liquid viscosity on horizontal stratified flow. Ph.D. Thesis, University of Illinois, Urbana-Champaign.

Andritsos, N., Hanratty, T., 1987. Influence of interfacial waves in stratified gas–liquid flows. AIChE J. 33, 444–454.

Barnea, D., Shoham, O., Taitel, Y., Dukler, A.E., 1980. Flow pattern transition for gas–liquid flow in horizontal and inclined pipes. Int. J. Multiphase Flow 6, 217–225.

Beggs, H.D., Brill, J.P., 1973. A study of two-phase flow in inclined pipes. J. Petrol. Technol., 607–617.

Biberg, D., 2002. Wall and interfacial friction in two-phase stratified pipe and channel flow. Tech. Rep., Institute of Energy Technology, Kjeller, Norway.

Bruno, K., McCready, M.J., 1988. Origin of roll waves in horizontal gas–liquid flows. AIChE J. 34, 1431–1440.

Cheremisinoff, N.P., Davis, E.J., 1979. Stratified turbulent–turbulent gas liquid flows. AIChE J. 25.

Cornish, V., 1934. Ocean Waves and Kindred Geophysical Phenomena. Cambridge University Press, London.

Espedal, M., 1998. An experimental investigation of stratified two-phase pipe flow at small inclinations. Ph.D. Thesis, NTNU, Trondheim, Norway.

Fan, Z., Ruder, Z., Hanratty, T.J., 1993. Initiation of slugs in horizontal gas–liquid flows. AIChE J. 39, 1741–1753.

Ferschneider, G., Lagiere, M., Bourgeois, T., Filtremann, M., 1985. How to calculate two-phase flow of gas and oil in pipe lines? Pipe Line Ind. 63, 33–39.

Haaland, S.E., 1983. Simple and explicit formulas for the friction factor in turbulent pipe flow. J. Fluids Eng. 105, 89–90.

Hanratty, T.J., 1991. Separated flow modelling and interfacial transport phenomena. Appl. Sci. Res. 48, 353–390.

Hanratty, T.J., Hershman, A., 1961. Initiation of roll waves. AIChE J. 7, 488–497.

Hurlburt, E.T., Hanratty, T.J., 2002. Prediction of the transition from stratified to slug and plug flows in long pipes. Int. J. Multiphase Flow 28, 707–729.

Johnson, G.W., Bertelsen, A., Nossen, J., 2009. A mechanistic model for roll wave for two-phase pipe flow. AIChE J. 55.

Kordyban, E.S., Ranov, T., 1970. Mechanism of slug formation in horizontal two-phase flow. J. Basic Eng. 92, 857–864.

Kowalski, J.E., 1987. Interfacial shear stress in stratified flow in a horizontal pipe. AIChE J. 33, 274–281.

Kristiansen, O., 2004. Experiments on the transition from stratified to slug flow in multiphase pipe flow. Ph.D. Thesis, Norwegian University of Science and Technology.

Lin, P.Y., Hanratty, T.J., 1986a. Prediction of the instability of slugs with linear stability theory. Int. J. Multiphase Flow 12, 79–98.

Miya, M., Woodmansee, D.E., Hanratty, T.J., 1971. A model for roll waves in gas–liquid flow. Chem. Eng. Sci. 26, 1915–1931.

Ruder, Z., Hanratty, P.H., Hanratty, T.J., 1989. Necessary conditions for the existence of stable slugs. JMP 18, 209–226.

Soleimani, A., Hanratty, T.J., 2003. Critical liquid flows for the transition from pseudo-slug and stratified patterns to slug flow. Int. J. Multiphase Flow 29, 51–67.

Strand, Ø., 1993. An experimental investigation of stratified two-phase flow in horizontal pipes. Ph.D. Thesis, University of Oslo.

Taitel, Y., Dukler, A.E., 1976. A model for predicting flow regime transitions in horizontal and near horizontal gas–liquid flow. AIChE J. 22, 47–55.

Wallis, G.B., Dobson, J.E., 1973. The onset of slugging in horizontal stratified air–water flow. Int. J. Multiphase Flow 1, 173–193.

Watson, M., 1989. Wavy stratified flow and the transition to slug flow. In: Multi-Phase Flow Proceedings of the Fourth International Conference BHRA, Bedford, UK, pp. 495–512.

Whitham, G.B., 1999. Linear and Nonlinear Waves. Wiley, New York.

Woods, B.D., 1998. Slug formation and frequency of slugging in gas–liquid flows. Ph.D. Thesis, University of Illinois, Urbana.

Woods, B.D., Hurlburt, E.T., Hanratty, T.J., 2000. Mechanism of slug formation in downwardly inclined pipes. Int. J. Multiphase Flow 26, 977–998.

Wu, H.L., Pots, B.F.M., Hollenberg, J.F., Meerhoff, R., 1987. Flow pattern transitions in two-phase gas/condensate flow at high pressure in an 8-inch horizontal pipe. In: Proceedings of the Third International Conference on Multi-Phase Flow. A2. BHRA, Cranfield, UK, The Hague, Netherlands, pp. 13–21.